THE ASTROPHYSICAL JOURNAL, 546:966–974, 2001 January 10

BROADBAND SPECTRAL ENERGY DISTRIBUTIONS OF ACTIVE GALACTIC NUCLEI FROM AN ACCRETION DISK WITH ADVECTIVE CORONAL FLOW

TOSHIHIRO KAWAGUCHI,[1,2] TOSHIYA SHIMURA,[3] AND SHIN MINESHIGE[1]
Received 2000 May 11; accepted 2000 August 25

ABSTRACT

Recent multiwaveband observations of Seyfert nuclei and QSOs established significant deviations in the spectral shape of the big blue bump from a blackbody spectral shape; soft X-ray excess has a spectral index α ($F_\nu \propto \nu^{-\alpha}$) of 1.6 and hard X-ray tail with α of ~ 0.7. We construct a disk-corona model which accounts for such broadband spectral properties. We study the emission spectrum emerging from a vertical disk-corona structure composed of two-temperature plasma by solving hydrostatic equilibrium and radiative transfer self-consistently. A fraction f of viscous heating due to mass accretion is assumed to be dissipated in a corona with a Thomson optical depth of τ_c, where advective cooling is also included, and a remaining fraction, $1-f$, dissipates within a main body of the disk. Our model can nicely reproduce the soft X-ray excess with a power-law shape and the hard tail extending to ~ 50 keV. The different spectral slopes ($\alpha \sim 1.5$ below 2 keV and ~ 0.5 above) are the results of different emission mechanisms and different sites; the former slope is due to unsaturated Comptonization from the innermost zone, and the latter is due to a combination of the Comptonization, bremsstrahlung, and a reflection of the coronal radiation at the disk-corona boundary from the inner to surrounding zone ($\lesssim 300$ Schwarzschild radii). The emergent optical spectrum is redder ($\alpha \sim 0.3$) than that of the standard disk ($\alpha \sim -0.3$), being consistent with observations, due to the different efficiencies of spectral hardening of disk emission at different radii. Further, we find that the cutoff frequency of the hard X-ray ($\sim$coronal electron temperature) and broadband spectral shape are insensitive to the black hole mass, while the peak frequency of the big blue bump is sensitive to the mass as the peak frequency $\propto M_{\rm BH}^{-1/4}$.

Subject headings: accretion, accretion disks — black hole physics — galaxies: active — galaxies: nuclei — radiation mechanisms: nonthermal

1. INTRODUCTION

Active galactic nuclei (AGNs) exhibit many spectral components over a wide waveband; an optical/ultraviolet (UV) bump, a power-law component in hard X-rays, an excess component in the soft X-ray band (so-called soft excess), a warm absorber feature around 1 keV in some objects, and a reflection/Fe Kα fluorescence line around a few to a few tens of keV (Mushotzky, Done, & Pounds 1993; Koratkar & Blaes 1999 for reviews). Those spectral components are commonly thought to be powered by gas accretion onto a massive black hole. The most well-known disk accretion model is called the standard disk model (Shakura & Sunyaev 1973). According to the standard disk model, the spectrum at each radius of the disk is assumed to be blackbody radiation with a local effective temperature, $T_{\rm eff}$. This simple picture was supported by the luminosity of the models and by rough agreement of optical/UV spectral energy distribution (SED) between observations and models (e.g., Shields 1978; Malkan & Sargent 1982).

The standard model, however, has limitations. (1) If UV turnover around 2000 Å is indeed an indication of the temperature at the innermost radius (e.g., Malkan 1983; Sun & Malkan 1989), such disks are too cool to produce enough soft X-ray photons. (2) Conversely, if the soft excess component at 0.1–1 keV is due to radiation from the innermost region, as is often assumed, such a disk only produces by 1.5–2 orders of magnitude less optical/UV flux than what is observed. (3) When optical and soft X-ray spectra are simultaneously fitted with the disk spectrum, the luminosity of the disks (L) often exceeds the Eddington luminosity ($L_{\rm Edd}$). (4) Observed optical spectra of QSOs are typically redder ($\alpha \sim 0.3$, where $L_\nu \propto \nu^{-\alpha}$; Francis et al. 1991) than those of the simplest standard accretion disks ($\alpha \sim -1/3$). In other words, a successful model spectrum of AGNs should deviate from that of the standard accretion disk. (5) Hard power-law X-ray cannot be reproduced.

A number of authors have tried to distort the disk spectrum toward the high-energy regime so that the disk can emit substantial soft X-ray and optical/UV radiation simultaneously. One promising idea is Comptonization within the disk in the vertical direction (Czerny & Elvis 1987; Wandel & Petrosian 1988; Laor & Netzer 1989; Ross, Fabian, & Mineshige 1992). The most accurate treatment of Comptonization in the framework of the standard model was made by Shimura & Takahara (1993, hereafter ST93), who solved radiative transfer and vertical structure simultaneously and presented emergent spectra integrated over radii (see also Shimura & Takahara 1995, hereafter ST95). The effect of Comptonization is more prominent at higher accretion rates (e.g., Ross et al. 1992; ST93; ST95).

However, there still remain discrepancies between models and observations. (1) Although Comptonization tends to increase α, the far-UV (FUV) spectra of these accretion disks exhibit $\alpha \sim 1$ at best when the luminosity of the disk approaches the Eddington limit (Ross et al. 1992; ST95). On the other hand, the observations of distant quasars showed steeper FUV spectra ($\alpha \sim 1.8$–2.2; Zheng et al. 1997). (2) The observed small spectral indices in soft X-ray ($\alpha \sim 1.4$–1.6; e.g., Walter & Fink 1993; Laor et al. 1997) are not

[1] Postal address: Department of Astronomy, Graduate School of Science, Kyoto University, Sakyo-ku, Kyoto 606-8502, Japan; kawaguti@kusastro.kyoto-u.ac.jp.
[2] Research Fellow of the Japan Society for the Promotion of Science.
[3] International Graduate School of Social Sciences, Yokohama National University, Hodogaya-ku, Yokohama 240-8501, Japan.

achieved by any disk models (e.g., Nandra et al. 1995 for Mrk 841; Laor et al. 1997 for a sample of low-redshift QSOs) because the higher energy tail of those disk models is the superposition of Wien laws, thus exhibiting exponential rollover. (3) These accretion disks still cannot reproduce the hard X-rays. Then hard X-ray emission should be treated as additional components in these models.

With these problems kept in mind, we, in this present study, aim to produce the overall SED simultaneously by disk-corona models. The spectrum to be reproduced with these models is a composite one obtained from several independent observations (see Zheng et al. 1997; Laor et al. 1997). It is composed of "typical" spectral indices over broadbands from near-IR to hard X-ray, optical–to–X-ray flux ratio, and the energy cutoff of the hard power-law component (see § 3.1 for a more detailed description). We can, for the first time, reproduce such broadband spectra. In § 2 we review the assumptions and numerical method used in the calculation. Numerical results and comparisons between the models and the composite spectrum are presented in § 3. The final section is devoted to discussion and summary.

2. BASIC ASSUMPTIONS AND EQUATIONS

The numerical code used in this study is basically the same as that of ST93 except for some modifications. We assume for the configuration of the system that the accretion disk main body is sandwiched between coronal layers in the vertical direction (e.g., Haardt & Maraschi 1991) and that the whole system is geometrically thin (i.e., plane-parallel slab geometry). We treat the disk-corona system consisting of fully ionized hydrogen, thermal plasma around a Schwarzschild black hole of mass $M_{\rm BH}$. Gas evaporation from the disk to corona and condensation from corona to disk (e.g., Meyer & Meyer-Hofmeister 1994) are not included here for simplicity; the disk and coronal layers are interacting only via radiation and pressure (e.g., Nakamura & Osaki 1993; Życki, Collin-Souffrin, & Czerny 1995). Although magnetic fields may also affect the disk-corona structures, they are not included in these calculations.

The equation of hydrostatic equilibrium in the vertical direction is given by

$$-\frac{dP_{\rm gas}}{dz}+\int_0^\infty dv\,\frac{F_v}{\lambda_v c}=m_p N_e \frac{GM_{\rm BH}}{R^3}\,z\,, \tag{1}$$

where R and z are the radial and the vertical coordinates, respectively, and $P_{\rm gas}$ and N_e are the gas pressure and the number density of electrons, respectively. For the radiation field, we adopt the diffusion approximation. Then the radiative flux F_v at some frequency v is given by

$$F_v=-\frac{c\lambda_v}{3}\left(\frac{\partial \epsilon_v}{\partial z}\right), \tag{2}$$

where ϵ_v and λ_v are the radiation energy density per unit frequency per unit volume and the mean free path of a photon with a frequency v, respectively. We set $\lambda_v=(\sigma_{\rm T}+\sigma_{{\rm ff},v})^{-1}N_e^{-1}$; we do not include the bound-free, free-bound, or bound-bound transitions in the calculations. Here $\sigma_{\rm T}$ and $\sigma_{{\rm ff},v}$ are the cross sections of Thomson scattering and bremsstrahlung absorption, respectively. The Thomson optical depth of the disk and corona measured from the midplane τ is related to the height from the midplane z as

$$d\tau=N_e\sigma_{\rm T}\,dz\,. \tag{3}$$

The total Thomson optical depth from the midplane (through the boundary between the disk and corona) to the surface of the corona, τ_0, is a free parameter. The equation of state is that $P_{\rm gas}=N_e k_{\rm B}(T_p+T_e)$, where T_p and T_e are temperature of protons and electrons, respectively.

The dissipated energy per unit surface area of the disk-corona system Q_0^+ in Newtonian approximation is written as (Shakura & Sunyaev 1973)

$$Q_0^+=\frac{3}{8\pi}\dot{M}\Omega_{\rm K}^2\left(1-\sqrt{3R_g/R}\right), \tag{4}$$

where $\dot{M}$ and $\Omega_{\rm K}$ $[=(GM_{\rm BH}/R^3)^{1/2}]$ are the total (above and below the midplane) accretion rate and the Keplerian angular velocity, respectively. The innermost radius of the disk-corona system is assumed to be $3R_g$, where R_g $[=2GM_{\rm BH}/c^2=3\times10^{13}\ (M_{\rm BH}/10^8\ M_\odot)\ {\rm cm}=0.01\ (M_{\rm BH}/10^8\ M_\odot)]$ lt-day is the Schwarzschild radius. For the case of a nonrotating black hole under nonrelativistic treatment, $\dot{M}=12L_{\rm Edd}/c^2$ $[=2.6\,(M_{\rm BH}/10^8\ M_\odot)M_\odot\ {\rm yr}^{-1}]$ corresponds to the accretion disk shining at $L_{\rm Edd}$ $[=1.3\times10^{46}\,(M_{\rm BH}/10^8\ M_\odot)\ {\rm ergs\ s}^{-1}]$.

A constant fraction f of mass accretion is assumed to be dissipated in the corona with a Thomson optical depth of τ_c, where advective energy transport of protons is also included in addition to radiative cooling of electrons (see Fig. 1). A remaining fraction, $1-f$, dissipates within the disk layer. Advection in the disk layer (i.e., slim disk model that will be discussed later) is not included because of small radial velocity there. The advective cooling rate in the corona per unit surface area, $Q_{\rm adv}^-$, is taken from the expression of optically thin advection-dominated accretion flow (ADAF) in the one-temperature case (i.e., $T_p=T_e$; see Kato, Fukue, & Mineshige 1998, p. 272):

$$Q_{\rm adv}^-=\frac{1}{16\pi^2}\left(\frac{\Omega_{\rm K}}{R^2}\right)\frac{(f\dot{M})^2\sigma_{\rm T}}{\alpha_c m_p \tau_c}\,. \tag{5}$$

Here α_c is the viscosity parameter which controls the efficiency of the advection in the corona. We perform numerical calculations under the condition that the advective cooling should be less than the dissipated energy in the coronal layer: $Q_{\rm adv}^-\le fQ_0^+$.

The heating rate in the disk and corona, q_d^+ and q_c^+, respectively, and advective cooling rate in the corona per unit volume, $q_{\rm adv}^-$, are assumed to be proportional to matter density at each site. As a result, the fraction of advective

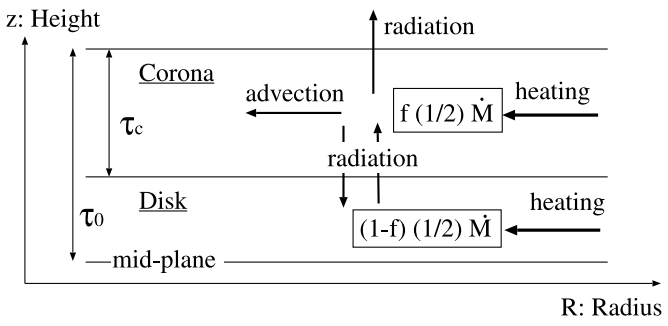

FIG. 1.—Schematic view of the energy balance in the present model

cooling in the dissipated energy is

$$\frac{q_{\rm adv}^-}{q_c^+} = \frac{Q_{\rm adv}^-}{fQ_0^+} = 0.21\left(\frac{f}{\alpha_c \tau_c}\right)\left(\frac{\dot{M}}{L_{\rm Edd}/c^2}\right) \times \left(\frac{R}{5R_g}\right)^{-1/2}\left(1-\sqrt{\frac{3R_g}{R}}\right)^{-1}. \quad (6)$$

The energy balance in each layer is as follows:

Disk: Protons: $q_d^+ = \lambda_{\rm ie}$, (7)

Electrons: $\lambda_{\rm ie} = \bar{q}_{\rm rad}$, (8)

Corona: Protons: $q_c^+ = q_{\rm adv}^- + \lambda_{\rm ie}$, (9)

Electrons: $\lambda_{\rm ie} = \bar{q}_{\rm rad}$, (10)

with

$$q_d^+ = (1-f)Q_0^+ \frac{\sigma_{\rm T} N_e}{\tau_0 - \tau_c}, \quad q_c^+ = fQ_0^+ \frac{\sigma_{\rm T} N_e}{\tau_c},$$

$$q_{\rm adv}^- = Q_{\rm adv}^- \frac{\sigma_{\rm T} N_e}{\tau_c}, \quad (11)$$

where $\lambda_{\rm ie}$ is the energy exchange rate due to Coulomb collisions taken from Guilbert & Stepney (1985) and $\bar{q}_{\rm rad}$ is the radiative cooling rate. We consider bremsstrahlung and Comptonization for emission mechanisms. Then radiative cooling rate $\bar{q}_{\rm rad}$ is described as

$$\bar{q}_{\rm rad} = \int d\nu(-cN_e \sigma_{{\rm ff},\nu}\epsilon_\nu + j_{{\rm ff},\nu} + j_{{\rm Comp},\nu}), \quad (12)$$

where $j_{{\rm ff},\nu}$ and $j_{{\rm Comp},\nu}$ are the bremsstrahlung emissivity (Rybicki & Lightman 1979) and the net rate of energy transfer from electrons to photons via Comptonization per unit volume per unit frequency, respectively. The latter is described by the Kompaneets equation (Rybicki & Lightman 1979; see Hua & Titarchuk 1995 for comparisons of the analytical treatment of Comptonization with Monte Carlo simulations). Thus, the radiative transfer equation for F_ν is written as

$$\frac{\partial F_\nu}{\partial z} = -cN_e \sigma_{{\rm ff},\nu}\epsilon_\nu + j_{{\rm ff},\nu} + j_{{\rm Comp},\nu}. \quad (13)$$

For the expression of the free-free absorption and emission ($\sigma_{{\rm ff},\nu}$ and $j_{{\rm ff},\nu}$, respectively), we take the Gaunt factor to be unity, for simplicity (see Rybicki & Lightman 1979).

Following ST93, we take ξ ($\equiv \log(\tau_0 - \tau)$) as an independent variable for the vertical coordinate. To calculate the spectra integrated over the whole disk (§ 3.1), we divide the disk-corona system from $3R_g$ to $300R_g$ into 20 concentric rings so that each ring radiates approximately the same luminosity (see Ross et al. 1992; ST95). In total, input free parameters required for the calculations are $M_{\rm BH}$, $\dot{M}$, f, τ_c, τ_0, and α_c. The number of these parameters is similar to that of relevant observed parameters which we aim to explain simultaneously, e.g., $L_{\rm X}$, $\alpha_{\rm ox}$, $\alpha_{\rm UV}$, $\alpha_{\rm opt}$, α_{ROSAT}, α_{ASCA}, and so on. Then outputs are $N_e(\xi)$, $T_e(\xi)$, $T_i(\xi)$, $P_{\rm gas}(\xi)$, $z(\xi)$, and $\epsilon_\nu(\xi)$. Spectrum of the whole disk-corona system is obtained by summing up the emergent spectra of all the rings.

The emergent spectrum at each ring does not so strongly depend on τ_0 as long as $\tau_0 \gg 1$ but is sensitive to τ_c. We thus take τ_0 as a constant over all rings, for simplicity. Currently, we do not have a good theory to predict the radial dependence of τ_c and f that can, in principle, be determined by physics of evaporation/condensation. Thus, τ_c and f are also simply assumed to be constant over all rings. The effects of changing τ_c and f will be discussed later.

General relativistic effects are not included. Since no Doppler broadening is considered, the total spectrum represents the case of a face-on disk. Convection/conductive energy transport is not included. Shakura, Sunyaev, & Zilitinkevich (1978) have shown that convection transports no more than $\sim 30\%$ of the vertical energy flux.

3. SPECTRAL ENERGY DISTRIBUTION OF AGNs

3.1. *Observed Composite Spectrum*

The spectrum to be reproduced with our models is a composite one (Fig. 2*a*, *dotted lines*), which is a useful probe for ascertaining whether a model for the SED of AGNs can work or not. The vertical normalization is determined so as to give rise to a representative optical luminosity among low-redshift quasars from the Bright Quasar Survey adopting $H_0 = 50$ km s^{-1} Mpc^{-1} and $q_0 = 0.5$ with an assumption of isotropic emission (see Laor et al. 1997). There are, however, two major problems that one should keep in mind when dealing with the composite spectrum (Koratkar & Blaes 1999; Laor 1999). (1) We observe objects with different redshifts in different wavebands; the spectral index in FUV is obtained from distant QSOs (Zheng et al. 1997), while that of the soft X-ray is mainly from nearby objects (e.g., Walter & Fink 1993; Laor et al. 1997). Also, the sample used in each waveband contains objects that are not necessarily the same objects. (2) Soft excess might be an instrumental/calibration problem; *BeppoSAX* observations did not detect soft X-ray excess in some objects, while excess was seen for the same objects with other telescopes (e.g., Matt 1999). Although the results are still controversial, we assume that soft excess really exists in most AGNs throughout this paper. In what follows, we try to reproduce broadband spectra similar to the composite one, as the first step.

3.2. *Model Spectrum Integrated over Radii*

We first show the most successful case with $M_{\rm BH} = 3 \times 10^9\, M_\odot$ and $\dot{M} = 0.5 L_{\rm Edd}/c^2$ that gives rise to luminosity of about 5% of the Eddington limit for a nonrotating black hole under nonrelativistic treatment. The solid line in Figure 2*a* shows an example of the resultant broadband spectra. Since the innermost ring from $3.0R_g$ to $4.0R_g$ does not satisfy the restriction that $q_{\rm adv}^-/q_c^+ \le 1.0$ for the parameter sets described in Figure 2*a*, we hereafter plot integrated spectra from $4.0R_g$ to $300R_g$. In other words, all dissipated energy is assumed to be carried out by advection in $3.0R_g < R < 4.0R_g$. To account for the radiation at the surfaces of coronae above and beyond the disk, the resultant spectrum is multiplied by 2. A significant fraction, $f = 0.6$, of mass accretion occurs at the corona. In this case, advective cooling in the corona is comparable with the radiative cooling at $R \sim 4.9R_g$; $q_{\rm adv}^-/q_c^+ \sim 0.5$ (eq. [6]). A spectrum of the standard disk with the same $M_{\rm BH}$ and $\dot{M}$ is also depicted for comparison (*dashed line*).

The presence of multiple spectral components is the most noteworthy feature of the present model. This is because different radiative mechanisms play roles in different wavebands in Figure 2*a*: thermal radiation of the disk in optical/UV, unsaturated Comptonization in FUV/soft X-ray, and a

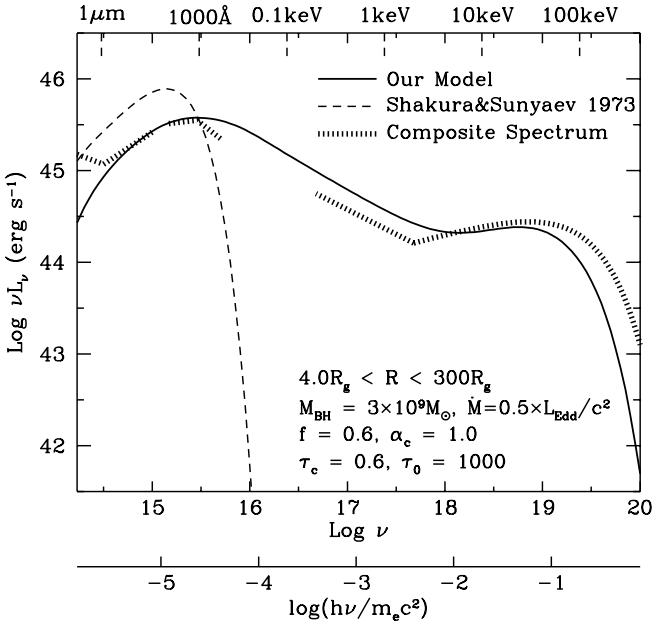

FIG. 2*a*

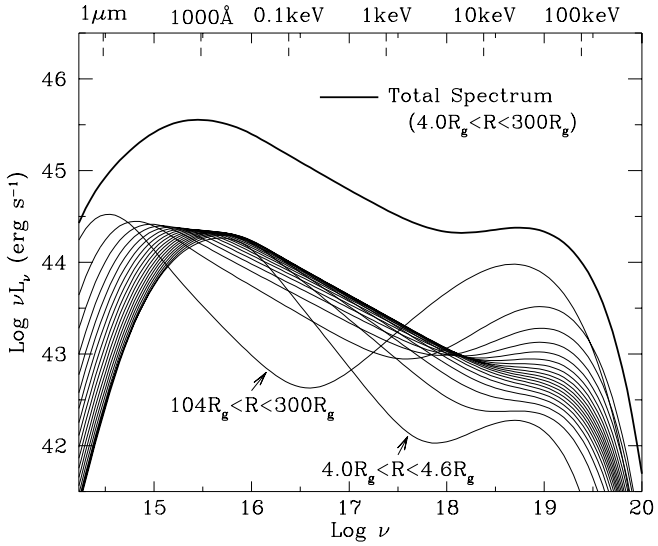

FIG. 2*b*

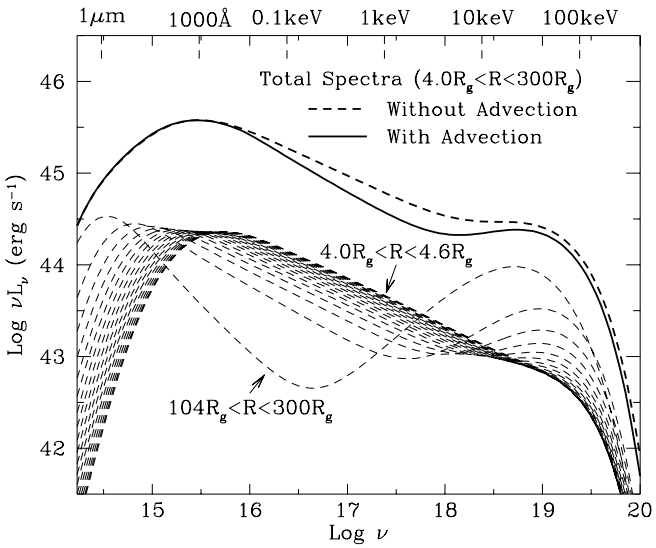

FIG. 2*c*

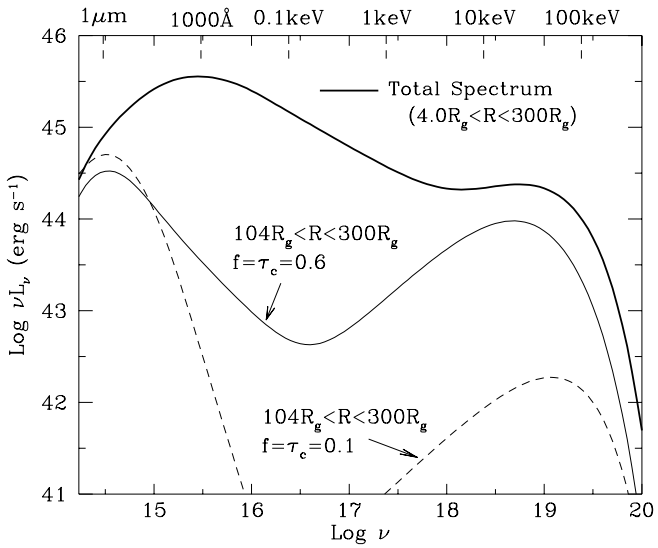

FIG. 2*d*

FIG. 2.—(*a*) Resultant spectrum from the disk-corona structure integrated over 4.0–300R_g (*heavy solid line*). Parameters used in this model are listed in the figure. With those parameter sets, advective cooling in the corona is comparable with the radiative cooling at $R \sim 4.9R_g$; $q_{\rm adv}^-/q_c^+ \sim 0.5$. Dashed line indicates the integrated spectra of the standard disk with the same $M_{\rm BH}$ and $\dot{M}$. Spectral indices of the observed composite spectra (*heavy dotted lines*) are α of 1.4 at NIR ($\lambda \geq 1$ μm), 0.3 at optical (1 μm $\geq \lambda \geq$ 2500 Å), 0.9 at UV (2500 Å $\geq \lambda \geq$ 1000 Å), 1.8 at FUV (1000 Å $\geq \lambda$), 1.6 at soft X-ray (0.2–2.0 keV), 0.7 at hard X-ray (>2.0 keV), 1.5 between optical and X-ray (2500 Å–2 keV). The energy cutoff for the hard X-ray power law is assumed to be 100 keV. (*b*) Contributions to the total spectrum due to individual rings (*lower curves*). Thick line denotes the total spectrum ($4.0R_g < R < 300R_g$) as the same as in (*a*). (*c*) The effect of advective cooling in the coronal layer to the emergent spectrum. Heavy dashed line is the resultant spectrum without advective cooling. Lower dashed curves represent contributions to the total spectrum due to each ring. Heavy solid curve has the same meaning as in (*a*) and (*b*). (*d*) Spectra for the outermost ring with $f = \tau_c = 0.6$ (*solid curve*) and $f = \tau_c = 0.1$ (*dashed curve*). It is shown that hard X-ray emission in the latter case is not strong as the former case, where bremsstrahlung emission at the outermost ring is the main origin of hardening in the total X-ray spectrum (*thick solid curve*; see [*b*]).

combination of the power-law component due to Comptonization, bremsstrahlung, and a reflection in hard X-ray. Note that the underlying radiative processes in soft–hard X-rays are distinct from those of the traditional explanation in which the UV–soft X-ray component is due to blackbody, whereas the hard power-law component is due to Comptonization of the soft photons. In our model, the hard X-ray spectrum appears to follow a power-law distribution with $\alpha \sim 0.5$–1.0 as a result of the combination of multiple radiative mechanisms, in contrast.

Figure 2*b* shows contributions to the total spectrum ($4.0R_g < R < 300R_g$; *solid line*) due to individual rings. The outermost ring ($104R_g < R < 300R_g$) contributes as much as one-third of the total spectrum at a few tens of keV. The usual models for X-ray emission of AGNs assume that only the inner region radiates X-rays (i.e., one zone); our model differs from the traditional model concerning the radial dependence of the X-ray spectrum, as well. Like optically thin ADAF (e.g., Narayan, Yi, & Mahadevan 1995; Manmoto, Mineshige, & Kusunose 1997), X-ray emission

arises from wide spatial range ($R \lesssim 300R_g$), in contrast with common belief. Interestingly, the contribution from the outer rings to the total X-ray spectrum decreases toward the lower energy X-ray band. Provided that inner rings are more time variable than outer rings, the resultant X-ray spectrum will get softer when the luminosity increases, as is actually observed (e.g., Done et al. 1995; Leighly et al. 1996). The most powerful test of our model will be gravitational microlensing (Yonehara et al. 1998) which provides information as to the size of emission region as a function of wavelength on AU ($\sim R_g$ for $10^8 M_{\rm BH}$) scales.

The effect of advective cooling in the coronal layer to the emergent spectrum is shown in Figure 2*c*. The wide dashed line is the resultant spectrum without advective cooling, which corresponds to a two-temperature treatment of the study by Shimura, Mineshige, & Takahara (1995), but with a constant τ_c. The lower dashed curves represent the spectra of each ring in the case without advective cooling. The heavy solid curve has the same meaning as in Figures 2*a* and 2*b*.

In our models above (Figs. 2*a*–2*c*), we assumed f and τ_c constant over all rings. This will be a reasonable assumption since Janiuk, Życki, & Czerny (2000), for example, estimated f as a function of the radius under some assumptions, finding that f is slowly increasing with the radius and that $0.2 < f < 1.0$ for various parameter sets at 3–$300R_g$. The coronal gas probably originates in evaporated gas accumulated in the flow (Meyer & Meyer-Hofmeister 1994; Liu, Meyer, & Meyer-Hofmeister 1997). In other words, we have assumed that a disk corona has already formed until $\sim 300R_g$. If, however, evaporation of disk material is still active at $R \lesssim 300R_g$, τ_c and f are both likely to increase with decreasing radius. To what extent the resultant spectrum changes in such a case is shown in Figure 2*d*. Spectra for the outermost ring with $f = \tau_c = 0.6$ (*solid curve*) and $f = \tau_c = 0.1$ (*dashed curve*) are shown. In the latter case, hard X-ray emission is not as strong as the former case, in which bremsstrahlung emission at the outermost ring is the main origin of hardening in the total X-ray spectrum (*heavy solid curve*). Then we are led to the conclusion that the corona must have developed until $300R_g$ so as to have large values of f and τ_c at the outermost ring, thereby reproducing the observed spectrum.

3.3. *Red Optical Spectrum*

The optical spectral index of QSOs has been recognized as a discrepancy between disk models and observations; Francis et al. (1991) reported that the bright QSOs, in which stellar contamination to the optical fluxes is relatively negligible, typically show a spectral index in the optical, α at 1500–5000 Å, of 0.32 ($L_\nu \propto \nu^{-\alpha}$), while the classical standard disk model predicts a spectral index of -0.33 (i.e., $L_\nu \propto \nu^{-1/3}$).

In order to emphasize the optical spectra, a part of Figure 2*a* is enlarged and shown in Figure 3 with additional spectra of disk models integrated over $3R_g < R < 1000R_g$. Heavy solid and dotted lines have the same meanings as in Figure 2*a*, and they both show a similar spectral index, $\alpha \sim 0.3$. The shaded area indicates the relevant waveband, 1500–5000 Å.

The reason why the current model has a better agreement with the observations in terms of the optical spectral index is as follows. The long-dashed line is a spectrum of the standard disk (i.e., eq. [4]), but without the inner boundary term (the term within parentheses on the right-hand side of eq. [4], which is sometimes omitted when roughly estimating the spectral index of the disk model). It shows $\alpha \sim -0.3$. Spectra of the standard disks with the inner boundary term are given by the short-dashed lines. The upper line represents the disk with $M_{\rm BH} = 3 \times 10^9\ M_\odot$ and $\dot{M} = 0.5 L_{\rm Edd}/c^2$, while the lower line is for $M_{\rm BH} = 10^8\ M_\odot$ and $\dot{M} = L_{\rm Edd}/c^2$, showing a somewhat redder spectrum ($\alpha \sim -0.1$) due to the inner boundary term.

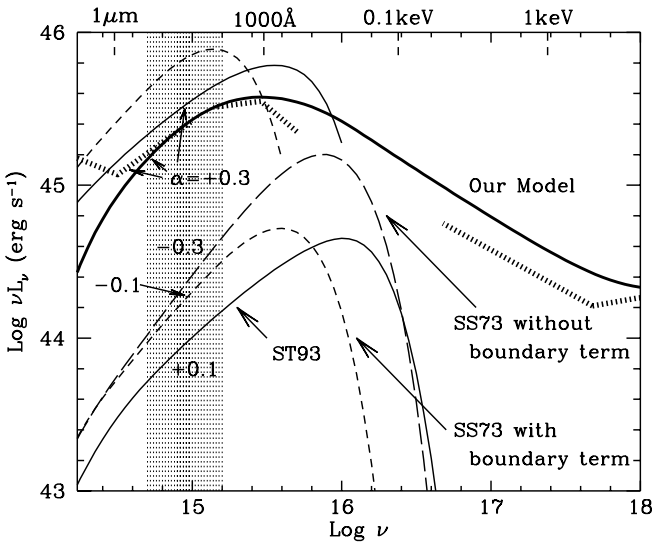

FIG. 3.—Spectra of various models with optical spectral indices α ($L_\nu \propto \nu^{-\alpha}$). The shaded area indicates the relevant waveband, 1500–5000 Å. Thick solid and dotted lines have the same meanings as in Fig. 2*a*. Spectra of the standard disks (Shakura & Sunyaev 1973; i.e., eq. [4]) are shown as the short-dashed lines as in Fig. 2*a*. A long-dashed one is calculated through eq. (4) without inner boundary term (the last term in eq. [4]). Finally, thin solid curves are obtained by radial integrations of the ST93 model (i.e., no corona). Lower three calculations are made for $M_{\rm BH} = 10^8\ M_\odot$ and $\dot{M} = L_{\rm Edd}/c^2$ at $3 < R < 1000R_g$, while upper two curves are for $M_{\rm BH} = 3 \times 10^9\ M_\odot$ and $\dot{M} = 0.5 L_{\rm Edd}/c^2$ at the same radii.

The emergent local spectrum changes its shape in the sense that the spectrum is distorted and shifted toward shorter wavelength when the electron scattering in the disk is taken into account (Czerny & Elvis 1987). Such a spectral shift is relatively more efficient in the inner region than in the outer region. As a result, disk models with electron scattering finally show redder optical spectra, $\alpha \sim 0.1$ in lower solid curve and $\alpha \sim 0.3$ in upper solid curve. The difference of spectral indices in the two solid curves, which are obtained by radial integrations of the ST93 model (i.e., no corona), are due mainly to the difference of their black hole masses. The disk with larger $M_{\rm BH}$ becomes cooler at fixed $\dot{M}/L_{\rm Edd}$ and R/R_g, as is expected for the standard accretion disk (eq. [14] described later). The optical band becomes a measure of the flux at the inner part of the disk, where it gets close to the edge of the integral interval (e.g., $3 < R < 1000R_g$). Then the emergent spectrum is somehow curved in the sense that it is redder than the spectrum from the outer region (e.g., Fig. 16 in Koratkar & Blaes 1999). Note that the redder spectra are achieved even within the framework of original ST93 and ST95 models, as well as our disk-corona model. If one wants to discuss the optical spectra in more detail, then heavy metals, bound-bound, free-bound, bound-free transitions, and a precise estimate of the contribution from the broad-line region (e.g., Balmer continuum) must be included.

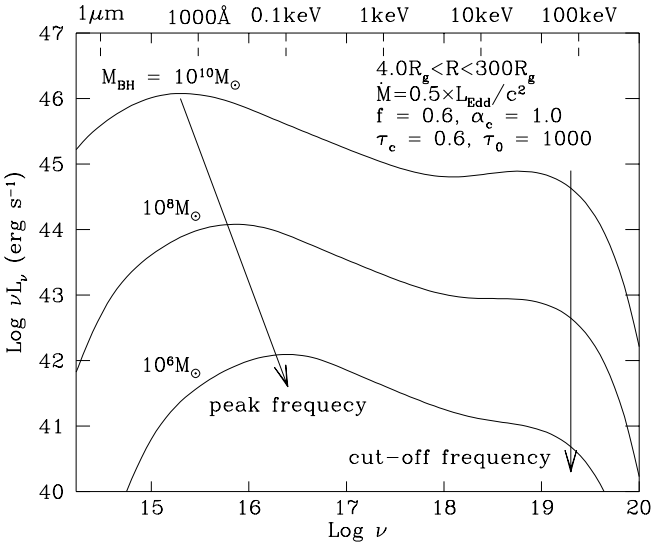

FIG. 4.—Black hole mass dependence of the emergent spectra with a fixed ratio of $\dot{M}$ to $L_{\rm Edd}$. Parameters used here are the same as those of Figs. 2*a* and 2*b*. The cutoff frequency of the hard X-ray (reflecting the coronal electron temperature) and X-ray spectral slopes are insensitive to the black hole mass, while the peak frequency of the big blue bump is sensitive to the mass.

3.4. *Spectra for Various $M_{\rm BH}$ and $\dot{M}$*

Figure 4 shows the black hole mass dependence of the spectra with a fixed ratio of $\dot{M}$ to $L_{\rm Edd}$ (i.e., fixed $\dot{M}/M_{\rm BH}$). The peak frequency of the big blue bump varies with $M_{\rm BH}$ in a fashion similar to that of the standard accretion disk in which

$$T_{\rm eff}(4R_g) \propto M_{\rm BH}^{-1/2}\dot{M}^{1/4} \propto M_{\rm BH}^{-1/4}(\dot{M}/L_{\rm Edd})^{1/4} . \quad (14)$$

On the other hand, the cutoff frequency of the hard X-ray (i.e., coronal electron temperature) and the spectral slopes in X-rays are rather insensitive to the black hole mass.

Accretion rate dependence of the emergent spectra with a fixed black hole mass ($M_{\rm BH} = 3 \times 10^9\ M_\odot$) is shown in Figure 5. The spectral slope at 0.1–2.0 keV stays almost constant, $\alpha = 1.46$, 1.58, and 1.62 for $\dot{M}/(L_{\rm Edd}/c^2) = 0.1$, 0.5, and 0.7, respectively.

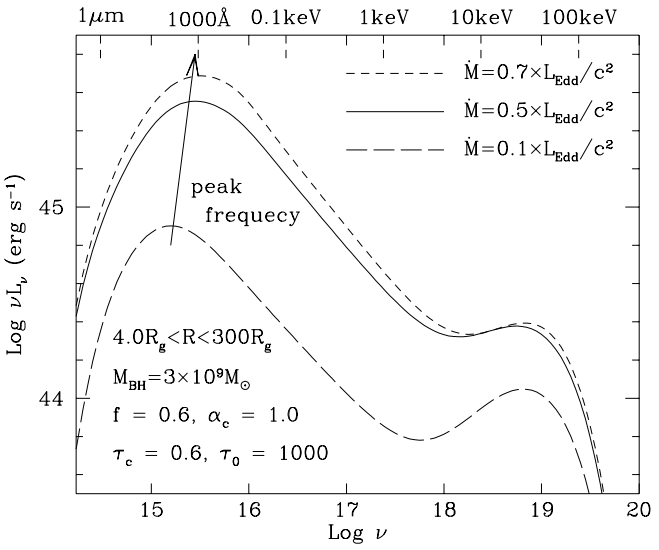

FIG. 5.—Accretion rate dependence of the emergent spectra with a fixed black hole mass ($M_{\rm BH} = 3 \times 10^9\ M_\odot$). The peak frequency of the big blue bump varies with $\dot{M}$ in a similar dependence for the case of standard accretion disk (eq. [14]).

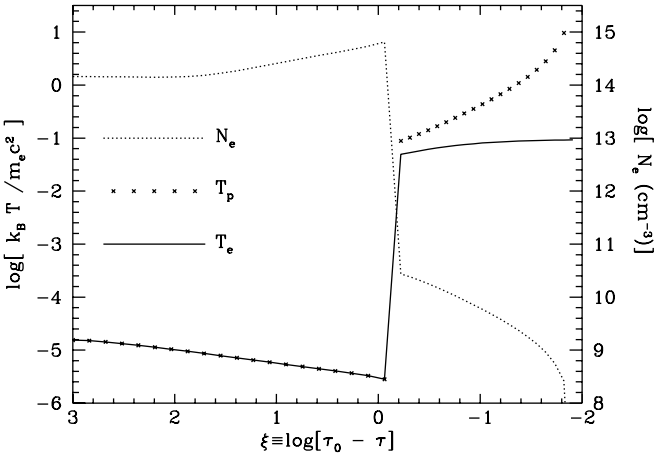

FIG. 6.—Vertical structure of the matter density (*dotted line*), proton temperature (*crosses*), and electron temperature (*solid line*). The midplane of the disk is located at ξ of 3, and the boundary between the disk and corona is at $\xi \sim -0.2$. It turns out that the height of the boundary measured from the midplane is $0.03R_g$, and that of the surface of the corona (at ξ of -2) is $0.3R_g$. Note that $k_{\rm B}T/m_e c^2 = 1$ corresponds to $T \simeq 5 \times 10^9$ K ($\simeq 500$ keV).

3.5. *Vertical Structure*

We finally present the vertical structure of the disk-corona system. The number density of electrons (*dotted line*) and temperature of protons (*crosses*) and electrons (*solid line*) at $R \sim 4.9R_g$ are shown in Figure 6. The left side of the figure where $\xi\ (\equiv \log(\tau_0 - \tau)) = 3$ corresponds to the midplane (i.e., $\tau_0 = 1000$), and the boundary between the disk and corona is located at $\xi \sim -0.2$ (i.e., $\tau_c = 0.6$). The parameters used here are the same as those of Figure 2*a*. It turns out that the height of the boundary measured from the midplane is $0.03R_g$ and that of the surface of the corona (at ξ of -2) is $0.3R_g$. Then the disk-corona system is indeed geometrically thin; the height of the corona from the midplane is $\lesssim 0.1R$.

4. DISCUSSION AND CONCLUSION

4.1. *Comparison with Previous Models*

The most widely accepted interpretation, to date, of soft and hard X-ray emission mechanisms is that soft excess is due to unscattered photons propagating from the disk-corona boundary to the coronal surface, while hard power-law emission is attributed to unsaturated Comptonization, i.e., photons that are Compton upscattered during the propagation within the corona. Monte Carlo simulations of propagating photons in the framework of two-zone treatment (disk and coronal layers) indeed reproduce a bumplike feature in soft X-ray and power-law component due to Comptonization in hard X-ray (e.g., Haardt & Maraschi 1991; Nakamura & Osaki 1993). However, the bumplike feature due to unscattered photons still keeps its spectral shape that it had at the disk-corona boundary even after it goes away from the coronal surface: i.e., it should look like blackbody radiation. The higher energy tail of the soft excess is predicted to be as steep as the Wien law, in contradiction with observed small spectral indices in soft X-ray ($\alpha \sim 1.4$–1.6).

Thermal bremsstrahlung emission was proposed for the hard X-ray power-law component by Schlosman, Shaham, & Shaviv (1984), where the emission comes from the disk-corona transition layer with a temperature gradient, and thermal conduction from the overlying corona is balanced with radiative cooling. They show that such a layer emits hard X-rays efficiently in the case of the accretion disk model proposed by Sakimoto & Coroniti (1981), in which viscous torque is proportional to gas pressure, but that it does not work in standard accretion disks where the torque is in proportion to the total pressure unless viscosity parameter in the disk is less than 10^{-3}. We should note here that nonthermal, power-law electron energy distribution models, similar to our results, produce two spectral power laws for soft and hard X-ray emission (e.g., Zdziarski & Lightman 1985), although ours is a thermal model.

Shimura et al. (1995) proposed a model in which FUV–hard X-ray is attributed to unsaturated Comptonization in a corona above a disk. Their claim is that their model, with τ_c a strongly increasing function of radius, reproduces a single power law in X-ray bands, not a broken power law (i.e., soft excess and hard power law). Then the corona could be patchy so that the disk is covered over only in part with the corona. In our model, however, bremsstrahlung emission from the corona and reflection of the coronal emission at the disk-corona boundary also contribute to hard X-ray as well as the unsaturated Comptonization. As a result, we have different spectral slopes at soft and hard X-ray bands. It largely depends on our assumption of constant f and τ_c. In other words, we need f and τ_c to be almost constant or weak functions of radius in order to expect sufficient bremsstrahlung emission from the corona at the outer region and then in order to reproduce the observed spectrum within the current framework. Theoretical work to check this assumption is needed as the next step. Without advective cooling in the corona, we also have rather straight spectrum from FUV to hard X-ray (see Fig. 2*c*). The effect of advection seems to bend the total spectrum so that the spectrum has two power laws in X-ray bands.

In the extremely high accretion rate, the disk spectra may be able to reproduce the observed steep spectral decline at 1000–400 Å, since Comptonization is more efficient at higher accretion rates and since an increase of accretion rate changes the disk dynamics from the standard disk to optically thick ADAF. Optically thick ADAF, which is the so-called slim disk model, radiates with higher temperature than the standard disk (Szuszkiewicz, Malkan, & Abramowicz 1996; Mineshige et al. 2000). Narrow-line Seyfert 1 galaxies (NLS1s) have peculiar spectral and temporal features that are not seen in normal Seyfert nuclei and QSOs (e.g., Boller, Brandt, & Fink 1996; Brandt, Mathur, & Elvis 1997; Leighly 1999a, 1999b; Grupe et al. 1998, 1999). These features are often attributed to small black hole mass and to high accretion rate (i.e., $L \sim L_{\rm Edd}$; e.g., Pounds, Done, & Osborne 1995; Hayashida et al. 1998; Mineshige et al. 2000). Then such extreme accretion rate is not relevant in this study, where we are going to construct a disk model for normal Seyfert galaxies/QSOs that perhaps have moderate accretion rate ($L \sim 0.01$–0.1 of $L_{\rm Edd}$; e.g., Wandel 1999). To account for systematically large α_{ROSAT} in NLS1s, we would need to reduce Compton-y-parameter in the corona.

The configuration of the cold ($\sim 10^5$ K) and hot (~ 100 keV) regions that radiate optical/UV bump and X-rays, respectively, is an unsolved problem. Optically thin ADAF is a possible energy source of X-ray emission. However, optically thin ADAF itself is basically faint (e.g., Mahadevan 1997) compared with observed luminosity of AGNs. Then the luminosity of the power-law X-ray emission indicates that cold material is located adjacent to such hot flow as a source of seed photons: for example, corona-like flows above and below a disk (e.g., Liang & Price 1977; Haardt & Maraschi 1991). Such a separation of a disk-corona system in the vertical direction has been also suggested from the stability of the disk with coronae against thermal and secular instabilities in the inner, radiation pressure–dominated region of the disk (Ionson & Kuperus 1984; Nakamura & Osaki 1993; Mineshige & Kusunose 1993), from the correlated variabilities between the iron-line flux and the X-ray continuum (e.g., Nandra et al. 1999; see also, however, Lee et al. 2000), and from the need for a cold disk as a "mirror" for reflection-component/broad-fluorescence line (e.g., Tanaka et al. 1995; Mushotzky et al. 1995; Nandra et al. 1997). Another potential problem is that those layers could be inhomogeneous and highly time dependent; the corona can be patchy (Shimura et al. 1995; Di Matteo 1998; Kawaguchi et al. 2000; Machida, Hayashi, & Matsumoto 2000), or the cold gas may exist as numerous blobs within the corona instead of the slab geometry (Guilbert & Rees 1988; Lightman & White 1988; Sivron & Tsuruta 1993; Collin-Souffrin et al. 1996; Krolik 1998; Różańska 1999). Nevertheless, spatially and temporally averaged treatment of the cold and hot regions will still be useful for study of time-averaged spectrum. Appropriate treatment of mass evaporation/condensation process is another future issue. In other words, f and τ_c may be variable in terms of R, $M_{\rm BH}$, $\dot{M}$. For instance, see Janiuk et al. (2000) for f as a function of R with various $\dot{M}$ values and viscosity parameters and Życki et al. (1995) for τ_c versus $\dot{M}$.

4.2. *Expected Time Variability*

Time variability provides strong constraints on spectral models. It is worthwhile to briefly comment on the temporal behavior, although we are now working on a model for the steady accretion disk-corona with an aim to reproduce the observed, time-averaged spectrum. The following are the qualitative arguments expected from our current model. More details are beyond the scope of this paper and will be reserved for future work.

For the optical-to-UV time lag observed in NGC 7469 (Wanders et al. 1997; Collier et al. 1998) and marginally detected in NGC 4151 (Peterson et al. 1998), our model can explain the lag as Collier et al. (1998) demonstrated using the standard accretion disk model. That is because the optical/UV emitter in our model is, like other spectral models, an accretion disk that has a similar dependence of (surface) temperature upon radius to the standard accretion disk. It should be noted here that such a time lag has not yet been established in all AGNs (Edelson et al. 2000).

Since the FUV, soft X-ray, and a part of hard X-ray emission come from the same region in our model, they are expected to vary without serious time lag (larger than an order of days), except for the difference of escaping (diffusion) time at different energies. Chiang et al. (2000) reported the interband lags in NGC 5548 from ~ 240 ks simultaneous observations; 0.14–0.18 keV flux leads 0.78 keV flux by ~ 10 ks and 5.4 keV flux by ~ 30 ks. As discussed in § 6 in their paper, these lags are consistent with a coronal size of $10R_g$ for a $10^8\ M_\odot$ black hole. Incidentally,

the black hole mass of NGC 5548 is estimated to be about $10^8\ M_\odot$ through the reverberation mapping method (Wandel, Peterson, & Malkan 1999; Kaspi et al. 2000). However, the $\sim$4 day X-ray lag behind UV near the peak flux levels and almost simultaneous variations near the minimum fluxes in NGC 7469 (Nandra et al. 1998) are not solved by our model easily, as well as other models, to date, fail to do.

Finally, our model qualitatively explains following two issues about spectral variability in X-rays on short timescales (less than months) that are reported by numerous X-ray observations (§ 3.2). (1) Soft X-ray flux is more variable than hard X-ray flux. (2) Hard X-ray becomes softer when it gets brighter.

4.3. *Conclusions*

We study emission spectrum emerging from the vertical disk-corona structure composed of two-temperature plasma by solving hydrostatic equilibrium and radiative transfer self-consistently. The key question is what physical condition exhibits a soft X-ray excess with a spectral index α ($F_\nu \propto \nu^{-\alpha}$) of 1.6 and a hard X-ray tail with α of 0.7 at the same time. In our model, a fraction f of viscous heating is assumed to be dissipated in a corona with a Thomson optical depth of τ_c, where advective cooling is also included, and the remaining fraction, $1-f$, dissipates within the main body of the disk. Our model can nicely reproduce the observed composite spectrum of AGNs, which shows soft X-ray excess with α of about 1.5 and hard tail extending to $\sim$50 keV with a different slope ($\alpha \sim 0.5$). Our model should be checked with individual objects in the future, though.

The broken power laws ($\alpha \sim 1.5$ below 2 keV and $\sim$0.5 above) are the results of different emission mechanisms: unsaturated Comptonization in soft X-rays and a combination of the Comptonization, bremsstrahlung, and a reflection of the coronal radiation at the disk-corona boundary in hard X-rays. Previous models, where soft X-ray excess is attributed to blackbody or saturated Comptonization of the disk blackbody, tended to deal with limited wavebands separately, while we tried to fit the broadband SED simultaneously. For that reason we have proposed emission mechanisms that are different from those of previous models, in soft and hard X-ray bands. Also, our model differs from the traditional models in the X-ray–emitting region: hard X-ray emission originates from a spatially spread region up to 300 Schwarzschild radii. The emergent optical spectrum is redder ($\alpha \sim 0.3$) than that of the standard disk ($\alpha \sim -0.3$), consistent with observations, due to the different efficiencies of spectral hardening (distortion and shift) of disk emission at different radii. The cutoff frequency of the hard X-ray (reflecting the coronal electron temperature) and X-ray spectral slopes are insensitive to the black hole mass, while the peak frequency of the big blue bump is sensitive to the mass.

We wish to thank Hitoshi Negoro for helpful discussions and encouragement and Makoto Kishimoto, Masaru Matsuoka, Karen Leighy, Juri Poutanen, Ken Ebisawa, and Lev Titarchuk for useful comments. We would also like to thank an anonymous referee for rewarding suggestions. T. K. is grateful to the organizers of the Guillermo Haro Advanced Lectures on the starburst-AGN connection held in 2000 in Mexico for the excellent lectures in that conference and acknowledges useful discussions with the participants, especially Dario Trevese and Agnieszka Janiuk. This work was supported in part by the Research Fellowship of the Japan Society for the Promotion of Science for Young Scientists (4616, to T. K.), and by the Grants-in-Aid of the Ministry of Education, Science, Sports and Culture of Japan (10640228, to S. M.).

REFERENCES

Boller, Th., Brandt, W. N., & Fink, H. H. 1996, A&A, 305, 53
Brandt, W. N., Mathur, S., & Elvis, M. 1997, MNRAS, 285, L25
Chiang, J., et al. 2000, ApJ, 528, 292
Collier, S. J., et al. 1998, ApJ, 500, 162
Collin-Souffrin, S., Czerny, B., Dumont, A.-M., & Życki, P. T. 1996, A&A, 314, 393
Czerny, B., & Elvis, M. 1987, ApJ, 321, 305
Di Matteo, T. 1998, MNRAS, 299, L15
Done, C., Pounds, K. A., Nandra, K., & Fabian, A. C. 1995, MNRAS, 275, 417
Edelson, R., et al. 2000, ApJ, 534, 180
Francis, P. J., Hewett, P. C., Foltz, C. B., Chaffee, F. H., Weymann, R. J., & Morris, S. L. 1991, ApJ, 373, 465
Grupe, G. D., Beuermann, K., Mannheim, K., & Thomas, H.-C. 1999, A&A, 350, 805
Grupe, G. D., Beuermann, K., Thomas, H.-C., Mannheim, K., & Fink, H. H. 1998, A&A, 330, 25
Guilbert, P. W., & Rees, M. J. 1988, MNRAS, 233, 475
Guilbert, P. W., & Stepney, S. 1985, MNRAS, 212, 523
Haardt, F., & Maraschi, L. 1991, ApJ, 380, L51
Hayashida, K., et al. 1998, ApJ, 500, 642
Hua, X.-M., & Titarchuk, L. 1995, ApJ, 449, 188
Ionson, J. A., & Kuperus, M. 1984, ApJ, 284, 389
Janiuk, A., Życki, P. T., & Czerny, B. 2000, MNRAS, 314, 364
Kaspi, S., Smith, P. S., Netzer, H., Maoz, D., Jannuzi, B. T., & Giveon, U. 2000, ApJ, 533, 631
Kato, S., Fukue, J., & Mineshige, S. 1998, Black-Hole Accretion Disks (Kyoto: Kyoto Univ. Press)
Kawaguchi, T., Mineshige, S., Machida, M., Matsumoto, R., & Shibata, K. 2000, PASJ, 52, L1
Koratkar, A., & Blaes, O. 1999, PASP, 111, 1
Krolik, J. H. 1998, ApJ, 498, L13
Laor, A. 1999, in ASP Conf. Ser. 162, Quasars and Cosmology, ed. G. Ferland & J. Baldwin (San Francisco: ASP), 341
Laor, A., Fiore, F., Elvis, M., Wilkes, B. J., & McDowell, J. C. 1997, ApJ, 477, 93
Laor, A., & Netzer, H. 1989, MNRAS, 238, 897
Lee, J. C., Fabian, A. C., Reynolds, C. S., Brandt, W. N., & Iwasawa, K. 2000, MNRAS, 318, 857
Leighly, K. M. 1999a, ApJS, 125, 297
———. 1999b, ApJS, 125, 317
Leighly, K. M., Kunieda, H., Awaki, H., & Tsuruta, S. 1996, ApJ, 463, 158
Liang, E. P. T., & Price, R. H. 1977, ApJ, 218, 247
Lightman, A. P., & White, T. R. 1988, ApJ, 335, 57
Liu, B. F., Meyer, F., & Meyer-Hofmeister, E. 1997, A&A, 328, 247
Machida, M., Hayashi, M., & Matsumoto, R. 2000, ApJ, 532, L67
Mahadevan, R. 1997, ApJ, 477, 585
Malkan, M. A. 1983, ApJ, 268, 582
Malkan, M. A., & Sargent, W. L. W. 1982, ApJ, 254, 22
Manmoto, T., Mineshige, S., & Kusunose, M. 1997, ApJ, 489, 791
Matt, G. 1999, in ASP Conf. Ser. 161, High Energy Processes in Accreting Black Holes, ed. J. Poutanen & R. Svensson (San Francisco: ASP), 149
Meyer, F., & Meyer-Hofmeister, E. 1994, A&A, 288, 175
Mineshige, S., Kawaguchi, T., Takeuchi, M., & Hayashida, K. 2000, PASJ, 52, 499
Mineshige, S., & Kusunose, M. 1993, PASJ, 45, 113
Mushotzky, R. F., Done, C., & Pounds, K. A. 1993, ARA&A, 31, 717
Mushotzky, R. F., Fabian, A. C., Iwasawa, K., Kunieda, H., Matusoka, M., Nandra, K., & Tanaka, Y. 1995, MNRAS, 272, L9
Nakamura, K., & Osaki, Y. 1993, PASJ, 45, 775
Nandra, K., et al. 1998, ApJ, 505, 594
Nandra, K., George, I. M., Mushotzky, R. F., Turner, T. J., & Yaqoob, T. 1997, ApJ, 477, 602
———. 1999, ApJ, 523, L17
Nandra, K., Turner, T. J., George, I. M., Fabian, A. C., Shrader, C., & Sun, W. H. 1995, MNRAS, 273, 85
Narayan, R., Yi, I., & Mahadevan, R. 1995, Nature, 374, 623
Peterson, B. M., Wanders, I., Horne, K., Collier, S., Tal, A., Kaspi, S., & Maoz, D. 1998, PASP, 110, 660
Pounds, K. A., Done, C., & Osborne, J. 1995, MNRAS, 277, L5
Ross, R. R., Fabian, A. C., & Mineshige, S. 1992, MNRAS, 258, 189
Różańska, A. 1999, MNRAS, 308, 751
Rybicki, G. B., & Lightman, A. P. 1979, Radiative Processes in Astrophysics (New York: Wiley)

Sakimoto, P. J., & Coroniti, F. V. 1981, ApJ, 247, 19
Schlosman, I., Shaham, J., & Shaviv, G. 1984, ApJ, 287, 534
Shakura, N. I., & Sunyaev, R. A. 1973, A&A, 24, 337
Shakura, N. I., Sunyaev, R. A., & Zilitinkevich, S. S. 1978, A&A, 62, 179
Shields, G. A. 1978, Nature, 272, 706
Shimura, T., Mineshige, S., & Takahara, F. 1995, ApJ, 439, 74
Shimura, T., & Takahara, F. 1993, ApJ, 419, 78 (ST93)
———. 1995, ApJ, 440, 610 (ST95)
Sivron, R., & Tsuruta, S. 1993, ApJ, 402, 420
Sun, W.-H., & Malkan, M. A. 1989, ApJ, 346, 68
Szuszkiewicz, E., Malkan, M. A., & Abramowicz, M. A. 1996, ApJ, 458, 474
Tanaka, Y., et al. 1995, Nature, 375, 659
Walter, R., & Fink, H. H. 1993, A&A, 274, 105
Wandel, A. 1999, ApJ, 527, 649
Wandel, A., Peterson, B. M., & Malkan, M. A. 1999, ApJ, 526, 579
Wandel, A., & Petrosian, V. 1988, ApJ, 329, L11
Wanders, I., et al. 1997, ApJS, 113, 69
Yonehara, A., Mineshige, S., Manmoto, T., Fukue, J., Umemura, M., & Turner, E. L. 1998, ApJ, 501, L41
Zdziarski, A. A., & Lightman, A. P. 1985, ApJ, 294, L79
Zheng, W., Kriss, G. A., Telfer, R. C., Grimes, J. P., & Davidsen, A. F. 1997, ApJ, 475, 469
Życki, P. T., Collin-Souffrin, S., & Czerny, B. 1995, MNRAS, 277, 70